

1 Geochemical mapping of a paleo-subduction zone beneath the 2 Troodos Ophiolite

3 *Dominic Woelki¹, Marcel Regelous¹, Karsten M. Haase¹, Christoph Beier¹

4 ¹GeoZentrum Nordbayern, Friedrich-Alexander-Universität (FAU) Erlangen-Nürnberg,

5 Schlossgarten 5, D-91054 Erlangen, Germany, dominic.woelki@fau.de

6 ABSTRACT

7 Supra-subduction zone ophiolites such as the Cretaceous Troodos Ophiolite of Cyprus
8 are fragments of oceanic crust formed by seafloor spreading close to subduction zones. Their
9 exact tectonic setting of origin has been intensively debated. Although many supra-subduction
10 zone ophiolites are thought to represent fore-arc crust, created during subduction initiation,
11 others may have formed at a subducting ridge, or in a back-arc, ridge-trench-trench/transform
12 triple junction or ‘plate edge’ setting. We carried out major and trace element analyses of 515
13 fresh volcanic glasses from 7 detailed sections through the Troodos lava sequence in order to
14 determine the regional and temporal variation in the composition of Troodos magmatism, and
15 hence reconstruct the distance and orientation of the Troodos spreading axis relative to the
16 former subduction zone. Troodos glasses range from boninite through tholeiitic basalt and
17 andesite to dacite. All glasses are enriched in fluid-mobile trace elements, and variably depleted
18 in the high-field strength elements compared to Mid-Ocean Ridge Basalt (MORB). None of
19 these glasses therefore have compositions identical to Izu-Bonin-Mariana fore-arc lavas that
20 have been proposed to be the prime example of lavas formed during subduction initiation.
21 Boninites are apparently restricted to the southern margin of the Troodos Ophiolite, and glasses
22 from the southeast margin of the ophiolite are the most depleted and contain the strongest input

1
2
3
4
5
6
7
8
9
10
11
12
13
14
15
16
17
18
19
20
21
22
23
24
25
26
27
28
29
30
31
32
33
34
35
36
37
38
39
40
41
42
43
44
45
46
47
48
49
50
51
52
53
54
55
56
57
58
59
60
61
62
63
64
65

23 of subduction zone fluid and melt signature. These geographic variations in glass composition
24 indicate that the Troodos Ophiolite formed by NW-SE directed spreading (at 91 Ma)
25 approximately 100 - 120 km above an eastward-dipping subducting plate. The orientation of the
26 Troodos spreading axis relative to the former trench could be explained if the Troodos Ophiolite
27 formed in a fore-arc position by subduction initiation at a transform fault. However, the lack of
28 glasses with fore-arc basalt composition, and similarities between the trace element compositions
29 of Troodos glasses and those from the Fonualei basin and northern Lau Basin in the southwest
30 Pacific suggest that the Troodos Ophiolite formed in a ridge-trench-trench or ridge-trench-
31 transform triple junction setting, at a back-arc spreading centre that propagated into arc and fore-
32 arc crust.

1. Introduction

Ophiolites yield important information on the structure and composition of the oceanic
crust and also provide insight into the evolution of large-scale plate tectonic processes. The
presence of a sheeted dyke complex, and the similarity to rock types dredged from the oceanic
crust implies that ophiolites were formed at oceanic spreading centres (Gass, 1968; Moores and
Vine, 1971). The geochemical compositions of lavas from ophiolites show that many formed
close to former subduction zones (Miyashiro, 1974; Pearce, 1975; Rautenschlein et al., 1985),
but the exact tectonic setting of formation of these 'supra-subduction zone' (SSZ) ophiolites is
debated. The presence of boninite lavas in some SSZ ophiolites has led to the perception that
they may represent slices of fore-arc crust and since fore-arc crust is thought to have formed
during subduction initiation, many SSZ ophiolites are assumed to record subduction initiation

1
2
3
4 45 events (Dilek and Furnes, 2009; Ishizuka et al., 2006; Pearce et al., 1984; Reagan et al., 2010;
5
6 46 Stern et al., 2012).

7
8
9 47 The lavas of the Cretaceous (approximately 91 Ma; (Mukasa and Ludden, 1987) Troodos
10
11 48 Ophiolite of Cyprus have been divided into an upper and lower pillow lava series, with boninitic
12
13
14 49 lavas apparently restricted to the upper pillow series (Pearce and Robinson, 2010). This
15
16 50 stratigraphic association of rock-types is thought to resemble that of the Izu-Bonin-Mariana
17
18 51 (IBM) fore-arc, where early fore-arc basalts are overlain by boninites, island arc tholeiitic lavas
19
20
21 52 and calc-alkaline arc deposits, recording the evolution from early spreading during subduction
22
23 53 initiation to a mature island arc (Ishizuka et al., 2014; Reagan et al., 2010). However, Woelki et
24
25 54 al. (2018) showed that on the southern margin of the Troodos Ophiolite, boninitic and tholeiitic
26
27
28 55 glasses are interbedded with no systematic change in composition with time. Other tectonic
29
30
31 56 models for the origin of the Troodos Ophiolite include formation at a subducting spreading ridge
32
33 57 (Osozawa et al., 2012), ridge-trench-trench or ridge-trench-transform triple junction (Regelous et
34
35
36 58 al., 2014; Woelki et al., 2018), rifted arc (Flower and Levine, 1987), or subduction initiation
37
38 59 plate edge setting (Pearce and Robinson, 2010). Distinguishing between these various models
39
40
41 60 requires a better understanding of the position of the former Troodos spreading axis to the
42
43 61 neighboring trench, and the temporal geochemical evolution of Troodos magmatism. Here, we
44
45 62 use geochemical data for lavas from stratigraphic sections through different parts of the ophiolite
46
47
48 63 to reconstruct the position of the ophiolite crust relative to the subducting slab.
49

50
51 64

52 53 65 **2. Samples and analytical methods**

54
55 66 In order to determine the spatial relationship between the former Troodos spreading
56
57
58 67 centre and the subduction zone, we examined the geographic and temporal variations in the
59
60
61
62
63
64
65

1
2
3
4 68 composition of lavas from the extrusive section of the Troodos Ophiolite. Hydrothermal
5
6 69 alteration of Troodos volcanic rocks has affected the concentrations of many of the fluid-mobile
7
8
9 70 trace elements that are distinctive of subduction-related lavas, however the chemical effects of
10
11 71 alteration on bulk lava compositions can be avoided by analysis of fresh volcanic glass using
12
13 72 microanalytical techniques. We measured the major and trace element compositions of 515 fresh
14
15 73 volcanic glasses, taken largely from seven detailed sections through the volcanic extrusive
16
17 74 sequence on both, the northern and southern margins of the ophiolite (Fig. 1, Table S1). These
18
19 75 sections cover much of the exposed volcanic extrusive series, and although the sections are not
20
21 76 entirely complete where fresh glass is lacking, most cover much of the 1000 - 1500 m thick
22
23 77 extrusive section (Figs. 1, 4). By analogy with fast-spreading oceanic crust (Brandl et al., 2016),
24
25 78 the period of time recorded in each volcanic section may be between 50 to 100 ky. Structural
26
27 79 orientations of the Troodos sheeted dykes are N-S to NW-SE (Maffione et al., 2017), thus lavas
28
29 80 from the northern and southern margins of the Troodos Ophiolite are of approximately the same
30
31 81 age, and all likely formed over a period of less than 2 My.

32
33 82 Glass samples were crushed and single 1-2 mm sized chips were hand-picked, cleaned in
34
35 83 distilled water, embedded in epoxy resin and polished for electron microprobe and laser-ablation
36
37 84 ICP-MS analyses. Fresh glasses (n = 515) from seven sections were analysed for major elements,
38
39 85 and 270 representative samples were selected for trace element analysis. Analysis of the major
40
41 86 elements (SiO₂, TiO₂, Al₂O₃, FeO_t, MnO, CaO, Na₂O, K₂O, P₂O₅, SO₃ and Cl) was carried out
42
43 87 using a JEOL JXA-8200 Superprobe electron microprobe at the GeoZentrum Nordbayern
44
45 88 (GZN), Friedrich-Alexander Universität Erlangen-Nürnberg, Germany. The microprobe was
46
47 89 operated with an acceleration voltage of 15 kV, a beam current of 15 nA and a defocused (10
48
49 90 µm) beam. Counting times were set to 20 s and 10 s for peaks and backgrounds for all elements,
50
51
52
53
54
55
56
57
58
59
60
61
62
63
64
65

1
2
3
4
5
6
7
8
9
10
11
12
13
14
15
16
17
18
19
20
21
22
23
24
25
26
27
28
29
30
31
32
33
34
35
36
37
38
39
40
41
42
43
44
45
46
47
48
49
50
51
52
53
54
55
56
57
58
59
60
61
62
63
64
65

91 except for Cl where peak counting time was 40 s and background times were set to 20 s.
92 Accuracy and precision were determined using international glass standards VG-2 and VG-A99
93 measured during each analytical session (Brandl et al., 2012). For the VG-A99 standard,
94 accuracy is better than 7.4 % for all elements except Cl, SO₃, and P₂O₅, and precision is better
95 than 4.7 % except for Cl, SO₃ and P₂O₅ (Beier et al., 2018). The average values of 10 spot
96 analyses on each sample are presented in Table S1.

97 Trace element concentrations of the glasses were determined by laser ablation inductively
98 coupled plasma mass spectrometry on the same glass fragments analysed for major elements,
99 using an Agilent 7500i quadrupole mass spectrometer coupled with a New Wave Research
100 UP193FX excimer laser at the GeoZentrum Nordbayern. A subset (n = 178) of the samples was
101 measured with a Teledyne Photon Machines Analyte Excite 193nm laser ablation system. The
102 beam diameter was set to 35 - 50 µm and the SiO₂ contents, previously determined by electron
103 microprobe, were used as internal standard. External calibration was performed using the
104 NIST614 glass standard. The international rock standard BCR-2g was measured to determine
105 accuracy and reproducibility. Accuracy was better than 13.1% except for Zn and Cu and
106 precision was better than 9.4% except for As and Cr. Repeat measurement of samples (n = 4)
107 with the newly established New Wave Research UP193FX excimer laser and the Teledyne
108 Photon Machines Analyte Excite 193nm laser yielded comparable values. Data in Table S1
109 represent averages of four individual analyses of each sample or standard. The new data
110 presented here are combined with published major and trace element data for Troodos glasses
111 from Akaki Canyon (Regelous et al., 2014) and Parekkklisia (Woelki et al., 2018) which were
112 measured in the same laboratory.

113

114 3. Results

115 Troodos volcanic glasses range in composition from high-Ca ($\text{CaO}/\text{Al}_2\text{O}_3 > 0.75$)
116 (Crawford et al., 1989) boninite (n=142), through tholeiitic basalt and andesite to dacite (n=373).
117 The MgO and TiO_2 contents of the glasses range from 10.7 to 0.3 wt% and 0.2 to 1.7 wt%,
118 respectively (Fig. 2). True boninitic glasses (with $\text{TiO}_2 < 0.5$ wt%, $\text{SiO}_2 > 52$ wt% and $\text{MgO} > 8$
119 wt%) occur exclusively on the southern margin of the ophiolite, but are not restricted to the
120 youngest part of the stratigraphy (Fig. 2, 4; Wölki et al., 2018). Highly evolved glasses with
121 $\text{MgO} < 2$ wt% were found only on the northern margin (Akaki, Peristerona and Kato Pyrgos)
122 (Fig. 2). The major element variations within glasses from individual sections are broadly
123 consistent with fractional crystallisation of olivine, olivine and clinopyroxene, or clinopyroxene
124 and plagioclase, which occur as microphenocrysts in the glasses. Incompatible trace element
125 ratios do not vary systematically with degree of magma differentiation, indicating that source
126 variations, rather than crystal fractionation or crustal assimilation are responsible for the range in
127 Troodos glass compositions (Fig. S1; König et al., 2010; Regelous et al., 2014; Woelki et al.,
128 2018).

129 Compared to MORB, most Troodos glasses were derived from more depleted mantle
130 sources (lower Zr/Yb). Ba/Th ratios of Troodos glasses are higher compared to MORB and range
131 from 78 to 270, overlapping with the composition of back-arc lavas from the Eastern Lau and
132 Fonualei Spreading Centres (Bézos et al., 2009; Escrig et al., 2012). All Troodos glasses have
133 relatively high concentrations of the fluid-mobile elements (Cs, Rb, Ba, U, Pb, Sr), with Ce/Pb
134 ratios (0.6 – 8.8) characteristic of subduction-related lavas (Fig. 3, 5). Correlations between
135 fluid-mobile and fluid-immobile trace element ratios (e.g. Ce/Pb and Zr/Yb) for glasses from
136 individual sections indicate that alteration has not affected the compositions of these samples

1
2
3
4
5
6
7
8
9
10
11
12
13
14
15
16
17
18
19
20
21
22
23
24
25
26
27
28
29
30
31
32
33
34
35
36
37
38
39
40
41
42
43
44
45
46
47
48
49
50
51
52
53
54
55
56
57
58
59
60
61
62
63
64
65

137 (Fig. 5). The mantle sources of the boninites and most depleted tholeiitic glasses have also been
138 enriched in Nb and Th by small-degree melts (König et al., 2010; Regelous et al., 2014; Woelki
139 et al., 2018) and display spoon-shaped rare-earth element patterns with La and Ce enrichments.
140 A detailed discussion of the petrogenesis of the Troodos glasses can be found in previous studies
141 (König et al., 2010; Osozawa et al., 2012; Rautenschlein et al., 1985; Regelous et al., 2014;
142 Woelki et al., 2018); here we focus on the stratigraphic and geographic variations in Troodos
143 glass compositions, and their significance in understanding the orientation of the former
144 subduction zone and the tectonic setting of ophiolite formation.

145 Despite the wide range in composition of Troodos glasses, the sections through the lavas
146 display no systematic change in composition with depth within the lava stratigraphy (Fig. 4).
147 Instead, our data show that the geochemical variations within Troodos glasses are primarily
148 related to their geographical location (Fig. 4, 5) rather than to relative stratigraphic age. Based on
149 trace element geochemistry, we divided the Troodos glasses into three major regions, the
150 northern margin (NM), the south-western margin (SWM), and the south-eastern margin (SEM;
151 Fig. 1). Glasses from the NM have relatively high and uniform Zr/Yb ratios (Fig. 4), whereas
152 those from the SWM are more depleted (lower Zr/Yb), and display a stronger fluid input, with
153 lower Ce/Pb and higher Ba/Ce ratios (see Fig. 4). The most depleted glasses are boninites and
154 tholeiites from the SEM in the vicinity of the Arakapas Transform Fault.

156 **4. Discussion**

157 **4.1. Comparison with fore-arc and back-arc lavas**

158 The lack of any systematic change in composition with relative stratigraphic age within
159 the Troodos lava pile contrasts with the geochemical evolution observed in the IBM fore-arc,

1
2
3
4 160 where the earliest lavas are fore-arc basalts which formed at short-lived spreading centres during
5
6 161 subduction initiation (Reagan et al., 2010) with no or minor subduction input (e.g., high Ce/Pb
7
8
9 162 ratios, Fig. 5). In the IBM fore-arc, the lavas become more depleted in high-field strength
10
11 163 elements and more enriched in light rare earth elements and fluid-mobile elements as subduction
12
13
14 164 proceeds. These intermediate lavas are typically overlain by boninites which record the highest
15
16 165 degree of mantle wedge depletion and enrichment by subduction zone components (Ishizuka et
17
18
19 166 al., 2018; Ishizuka et al., 2014; Reagan et al., 2010; Reagan et al., 2017; Whattam and Stern,
20
21 167 2011). In contrast, none of our sections through the Troodos lavas exhibits a trend to more
22
23
24 168 depleted, more fluid-enriched compositions with time. More recent drilling of the IBM fore-arc
25
26 169 indicates that boninites may in fact be restricted to the shallower side of the fore-arc, with fore-
27
28
29 170 arc basalts located closer to the trench (Pearce et al., 2015). However, in Troodos there are no
30
31 171 glasses with Ce/Pb ratios >8 that characterise many fore-arc basalts (Fig. 5), and most Troodos
32
33 172 glasses were derived from a highly depleted mantle source (low Zr/Yb), suggesting that the
34
35
36 173 subduction zone existed during the entire spreading stage exposed in the Troodos Ophiolite.
37
38 174 Low-Ca boninites from the IBM fore-arc have high Zr and Hf concentrations relative to Sm and
39
40
41 175 Eu (Fig. 3), unlike the high-Ca boninitic glasses from the Troodos Ophiolite. High-Ca boninites
42
43 176 without the association of low-Ca boninites are known from the northern termination of the
44
45
46 177 Tonga trench and the southern termination of the Vanuatu Trench (Danyushevsky et al., 1995;
47
48 178 Falloon et al., 1987; Sharaskin et al., 1983; Sigurdsson et al., 1993). These two areas represent
49
50
51 179 special tectonic settings where the trench terminates into a transition zone of transform tectonics,
52
53 180 and a back-arc spreading centre propagates into the fore-arc region, respectively (Falloon and
54
55 181 Crawford, 1991; Sigurdsson et al., 1993).

1
2
3
4
5
6
7
8
9
10
11
12
13
14
15
16
17
18
19
20
21
22
23
24
25
26
27
28
29
30
31
32
33
34
35
36
37
38
39
40
41
42
43
44
45
46
47
48
49
50
51
52
53
54
55
56
57
58
59
60
61
62
63
64
65

182 The compositional range of the lavas and the magmatic evolution of the Troodos
183 Ophiolite is thus very different from that inferred for the IBM fore-arc crust.

184 Instead, the variably depleted and fluid-mobile element enriched compositions of
185 Troodos glasses are similar to those recovered from back-arc and rear-arc spreading centres. In
186 Fig. 5 and 6, we compare the compositions of Troodos glasses with those from active spreading
187 centres in the Tonga arc - Lau back-arc basin in the western Pacific, which are located at varying
188 distance to the active Tonga arc, and from which fresh volcanic glasses have been recovered
189 (Bach et al., 1998; Bézoz et al., 2009; Caulfield et al., 2012a; Escrig et al., 2012; Keller et al.,
190 2008; Pearce et al., 1994; Peate et al., 2001).

191 In Fig. 5 the NM glasses lie on an array between MORB compositions and arc front lavas
192 from Tofua Island, overlapping with back-arc basin basalts of the Fonualei Spreading Centre
193 (FSC) in the Lau Basin (Fig. 5). The more depleted SWM glasses partly overlap with arc lavas of
194 Tofua Island but extend to lower Zr/Yb and Ce/Pb, indicating higher degrees of mantle depletion
195 and high addition of subduction zone fluid. The SEM glasses are less enriched in fluid-mobile
196 elements but were derived from a depleted mantle source, and overlap in composition with
197 Tonga arc boninites (Fig. 5). The mean composition of 142 Troodos boninitic glasses is similar
198 in composition to young boninites recovered from the Tonga arc and rear-arc (Cooper et al.,
199 2010; Falloon and Crawford, 1991; Falloon et al., 2008; Falloon et al., 2007; Falloon et al.,
200 1989) (Fig. 3). In conclusion, the Troodos glasses have more similarities with Tonga back-arc
201 lavas, than to lavas found in the IBM fore-arc crust.

202

1
2
3
4
5
6
7
8
9
10
11
12
13
14
15
16
17
18
19
20
21
22
23
24
25
26
27
28
29
30
31
32
33
34
35
36
37
38
39
40
41
42
43
44
45
46
47
48
49
50
51
52
53
54
55
56
57
58
59
60
61
62
63
64
65

203 **4.2. Geochemical mapping of the former subduction zone**

204 Previous studies have shown that within the Lau Basin, back-arc lava compositions vary
205 systematically with distance to the active arc front (Bach et al., 1998; Bézou et al., 2009; Escrig
206 et al., 2012; Keller et al., 2008; Pearce et al., 1994; Peate et al., 2001). The geographic variations
207 in Troodos glass compositions and their geochemical similarities to lavas from the active Tonga-
208 Lau subduction system therefore allow us to reconstruct the location and orientation of the
209 former subduction zone beneath the Troodos Ophiolite.

210 The more depleted and greater fluid enrichment of the glasses from the southern margin
211 of the Troodos Ophiolite indicate that at 91 Ma, the southern section of the Troodos spreading
212 centre was located closer to the trench. The absolute distance from the trench can be estimated
213 by comparison with lavas from spreading centres in the active Tonga – Lau Basin arc – back-arc
214 system. The overlap in composition between the NM glasses and the back-arc lavas from the
215 Fonualei Spreading Centre suggests that ~91 Ma ago the northern margin of Troodos may have
216 been located at a similar distance above the subducting slab as the recent Fonualei Spreading
217 Centre (Fig. 5, 6). The lavas of the Fonualei Spreading Centre erupted close (25 – 75 km) to the
218 active Tofua arc, 175 – 225 km from the Tonga trench, and approximately 125 – 177 km above
219 the subducting slab (Caulfield et al., 2012a; Escrig et al., 2012; Keller et al., 2008). The SEM
220 and SWM glasses were therefore located 30 – 40 km closer to the trench, in an arc or fore-arc
221 position, and by analogy with modern arcs, approximately 100 - 110 km above the subducting
222 plate (Syracuse and Abers, 2006). The very low Zr/Yb ratios of the Troodos SEM and SWM
223 glasses, which are unlike any modern Tonga-Lau or IBM fore-arc lavas, can be explained by the
224 location of the spreading centre in an arc or fore-arc position (Fig. 6), underlain by mantle which
225 was highly depleted by previous melting events, together with high degrees of melting due to

1
2
3
4
5
6
7
8
9
10
11
12
13
14
15
16
17
18
19
20
21
22
23
24
25
26
27
28
29
30
31
32
33
34
35
36
37
38
39
40
41
42
43
44
45
46
47
48
49
50
51
52
53
54
55
56
57
58
59
60
61
62
63
64
65

upwelling and melting of hydrous mantle at shallow levels beneath the spreading centre (Flower and Levine, 1987; Moores et al., 1984). In such a position, the arc magmatism would be captured by the overlying spreading centre. The distribution of Troodos glasses in the $Fe_8 - Ti_8$ diagram (Fig. 7) supports this interpretation. NM glasses (e.g. Akaki) define positive arrays in this diagram, overlapping with back-arc basin basalts of the Eastern Lau Spreading Centre but extending to more depleted (lower Fe_8 and Ti_8) values, consistent with mixing of melts from ‘wet’ and ‘damp’ moderately depleted mantle sources (Le Voci et al., 2014). SEM and SWM glasses were derived from depleted and highly depleted wet mantle sources and overlap with Fonualei back-arc lavas (Fig. 7). In conclusion, the Troodos glasses display a greater mantle wedge depletion and higher input of a subduction zone component from north to south, indicating a closer position for the SWM and SEM glasses to the trench.

The Troodos Ophiolite has been rotated 90° anticlockwise since its formation (Clube et al., 1985), thus we infer that at 91 Ma, the Troodos spreading axis was located about 100 – 120 km above an eastward dipping subducting plate (Fig. 8) within the former Tethys Ocean. The relatively high (approximately 45°) angle between the former trench (N-S, as determined from our analyses), and the Cretaceous paleo-spreading axis (E-W to NE-SW, on the basis of sheeted dyke orientations (Maffione et al., 2017), may explain the steep along-axis geochemical gradients observed in the Troodos glasses.

4.3. Geodynamic setting of formation of the Troodos Ophiolite

Our major and trace element data, in particular the enrichment in fluid-soluble elements (Rb, Cs, U, Pb, Ba) for fresh, unaltered volcanic glasses from the Troodos Ophiolite confirm its formation in a “supra-subduction zone” setting, as previously reported by many workers (Pearce

1
2
3
4
5
6
7
8
9
10
11
12
13
14
15
16
17
18
19
20
21
22
23
24
25
26
27
28
29
30
31
32
33
34
35
36
37
38
39
40
41
42
43
44
45
46
47
48
49
50
51
52
53
54
55
56
57
58
59
60
61
62
63
64
65

249 and Robinson, 2010; Rautenschlein et al., 1985; Regelous et al., 2014; Robinson et al., 2003;
250 Robinson et al., 1983; Woelki et al., 2018). The more depleted trace element compositions, lower
251 Ce/Pb and the presence of boninites suggest that the Troodos spreading axis was located closer
252 to the trench than most currently-active back-arc spreading centres, in an arc or fore-arc position.

253 In many models of subduction initiation, the spreading centres at which fore-arc crust
254 was accreted are presumed to have been oriented parallel to the trench (Pearce et al., 2015). The
255 high angle between the former trench and the Troodos spreading axis inferred from our data is
256 incompatible with such a model, but could possibly be explained by models of subduction
257 initiation in which a trench initiates within oceanic crust at a transform fault (e.g. (Casey and
258 Dewey, 1984). However, as discussed above, fluid-enriched compositions of all Troodos glasses
259 and the extremely low Zr/Yb in the most depleted glasses suggest that the Troodos crust formed
260 above an existing subduction zone, rather than during subduction initiation.

261 The geometry we infer for the former Troodos ridge-trench system is also inconsistent
262 with some previous models for the geodynamic setting of the Troodos Ophiolite. Osozawa et al.
263 (2012) argued for ridge subduction shortly after subduction initiation. However, the depleted
264 compositions of Troodos glasses, with $Zr/Yb < MORB$ and higher contribution of a slab
265 component ($Ce/Pb < 10$), are unlike those from the subducting segments of the Chile Rise closest
266 to the South American Trench ($Ce/Pb > 16$) (Karsten et al., 1996). As previously suggested
267 (Flower and Levine, 1987; Moores et al., 1984; Regelous et al., 2014; Woelki et al., 2018), we
268 conclude that the Troodos Ophiolite formed at a ridge-trench-trench (RTT) or ridge-trench-
269 transform (RTF) triple junction, where previously depleted, fluid-enriched mantle above the
270 subducting slab underwent extensive melting beneath the spreading axis. This setting is similar

1
2
3
4
5
6
7
8
9
10
11
12
13
14
15
16
17
18
19
20
21
22
23
24
25
26
27
28
29
30
31
32
33
34
35
36
37
38
39
40
41
42
43
44
45
46
47
48
49
50
51
52
53
54
55
56
57
58
59
60
61
62
63
64
65

271 to the trench-transform ‘plate-edge’ setting of Pearce and Robinson (2010), but without
272 appealing to subduction initiation.

273 Such tectonic settings are rare on Earth today, but present-day equivalents may include
274 the southern North Fiji Basin (intersection of the Central North Fiji Basin spreading centre with
275 the Hunter Fracture Zone and the Southern Vanuatu Trench) and the northern Tonga Arc – Lau
276 Basin (intersection of the Northeast Lau Spreading Centre and the Vitiaz – Tonga Trench). In
277 both locations, young, predominantly high-Ca boninites have been reported (Crawford et al.,
278 1981; Crawford et al., 1989; Danyushevsky et al., 1995; Resing et al., 2011; Sigurdsson et al.,
279 1993), which are unrelated to subduction initiation. Upwelling of previously-depleted, fluid-
280 enriched mantle to shallow levels beneath a spreading centre close to a trench can explain the
281 highly depleted compositions of Troodos glasses which have few modern equivalents, and
282 possibly also the higher temperature of alteration of Troodos crust compared to oceanic crust
283 (Alt and Teagle, 2000; Crawford et al., 1989; Falloon and Crawford, 1991). More detailed
284 sampling of these young boninitic lavas are needed to test this model.

285 Ridge-trench-trench (RTT) and ridge-trench-transform (RTF) triple junctions may be
286 stable plate tectonic configurations (McKenzie and Morgan, 1969) that can nevertheless
287 propagate rapidly laterally, which could explain the similar age of many Tethyan “supra-
288 subduction zone” ophiolites (Troodos, Oman, Kizildag – 91-95 Ma, (Mirdita-Vourinos-Crete-
289 Pindos = 165-164-170-171 Ma) (Dilek and Flower, 2003; Dilek and Thy, 2009; Robertson,
290 2002). A spreading centre at an RTT or RTF triple junction will ‘capture’ the adjacent arc
291 magmatism, which can explain the lack of overlying arc volcanics on Troodos and many other
292 Tethyan ophiolites. Young, buoyant oceanic crust created on the over-riding plate close to a
293 subduction zone will be particularly susceptible to obduction and preservation. Despite their

1
2
3
4
5
6
7
8
9
10
11
12
13
14
15
16
17
18
19
20
21
22
23
24
25
26
27
28
29
30
31
32
33
34
35
36
37
38
39
40
41
42
43
44
45
46
47
48
49
50
51
52
53
54
55
56
57
58
59
60
61
62
63
64
65

294 present rarity, these tectonic settings are therefore particularly efficient sites for SSZ ophiolite
295 production and preservation.

296

297 **Acknowledgments**

298 We thank the Smithsonian Institution for providing electron microprobe standards, and Helene
299 Brätz and Reiner Klemd for help with LA-ICP-MS analyses. We acknowledge Peter Michael for
300 useful discussions, and Patrick Hoyer and Julia Bauer for help in the field. This research was
301 funded by the Deutsche Forschungsgemeinschaft grant RE3020/11-1.

302 **References**

303 Alt, J. C., and Teagle, D. A., 2000, Hydrothermal alteration and fluid fluxes in ophiolites and
304 oceanic crust: Special Papers-Geological Society of America, p. 273-282.
305 Bach, W., Hegner, E., and Erzinger, J., 1998, Chemical fluxes in the Tonga subduction zone:
306 Evidence from the southern Lau Basin: Geophysical Research Letters, v. 25, no. 9, p.
307 1467-1470.
308 Beier, C., Brandl, P. A., Lima, S. M., and Haase, K. M., 2018, Tectonic control on the genesis of
309 magmas in the New Hebrides arc (Vanuatu): Lithos, v. 312, p. 290-307.
310 Bézou, A., Escrig, S., Langmuir, C. H., Michael, P. J., and Asimow, P. D., 2009, Origins of
311 chemical diversity of back- arc basin basalts: A segment- scale study of the Eastern Lau
312 Spreading Center: Journal of Geophysical Research: Solid Earth, v. 114, no. B6.
313 Brandl, P. A., Regelous, M., Beier, C., O'Neill, H. S. C., Nebel, O., and Haase, K. M., 2016, The
314 timescales of magma evolution at mid-ocean ridges: Lithos, v. 240, p. 49-68.
315 Casey, J., and Dewey, J., 1984, Initiation of subduction zones along transform and accreting
316 plate boundaries, triple-junction evolution, and forearc spreading centres—implications
317 for ophiolitic geology and obduction: Geological Society, London, Special Publications,
318 v. 13, no. 1, p. 269-290.
319 Caulfield, J., Turner, S., Arculus, R., Dale, C., Jenner, F., Pearce, J., Macpherson, C., and
320 Handley, H., 2012a, Mantle flow, volatiles, slab- surface temperatures and melting
321 dynamics in the north Tonga arc–Lau back- arc basin: Journal of Geophysical Research:
322 Solid Earth, v. 117, no. B11.
323 Caulfield, J., Turner, S. P., Smith, I., Cooper, L., and Jenner, G. A., 2012b, Magma evolution in
324 the primitive, intra-oceanic Tonga arc: petrogenesis of basaltic andesites at Tofua
325 volcano: Journal of petrology, v. 53, no. 6, p. 1197-1230.
326 Clube, T. M. M., Creer, K., and Robertson, A., 1985, Palaeorotation of the Troodos microplate,
327 Cyprus: Nature, v. 317, no. 6037, p. 522.
328 Constantinou, G., 1995, Geological map of Cyprus: Geological Survey Department, Cyprus.

1
2
3
4
5
6
7
8
9
10
11
12
13
14
15
16
17
18
19
20
21
22
23
24
25
26
27
28
29
30
31
32
33
34
35
36
37
38
39
40
41
42
43
44
45
46
47
48
49
50
51
52
53
54
55
56
57
58
59
60
61
62
63
64
65

329 Cooper, L. B., Plank, T., Arculus, R. J., Hauri, E. H., Hall, P. S., and Parman, S. W., 2010,
330 High- Ca boninites from the active Tonga Arc: *Journal of Geophysical Research: Solid*
331 *Earth*, v. 115, no. B10.

332 Crawford, A. J., Beccaluva, L., and Serri, G., 1981, Tectono-magmatic evolution of the West
333 Philippine-Mariana region and the origin of boninites: *Earth and Planetary Science*
334 *Letters*, v. 54, no. 2, p. 346-356.

335 Crawford, A. J., Falloon, T., and Green, D., 1989, Classification, petrogenesis and tectonic
336 setting of boninites: *Boninites and related rocks*, p. 1-49.

337 Danyushevsky, L. V., Sobolev, A. V., and Falloon, T. J., 1995, North Tongan high-Ca boninite
338 petrogenesis: The role of Samoan plume and subduction zone-transform fault transition:
339 *Journal of Geodynamics*, v. 20, no. 3, p. 219-241.

340 Dilek, Y., and Flower, M. F., 2003, Arc-trench rollback and forearc accretion: 2. A model
341 template for ophiolites in Albania, Cyprus, and Oman: *Geological Society, London,*
342 *Special Publications*, v. 218, no. 1, p. 43-68.

343 Dilek, Y., and Furnes, H., 2009, Structure and geochemistry of Tethyan ophiolites and their
344 petrogenesis in subduction rollback systems: *Lithos*, v. 113, no. 1, p. 1-20.

345 Dilek, Y., and Thy, P., 2009, Island arc tholeiite to boninitic melt evolution of the Cretaceous
346 Kizildag (Turkey) ophiolite: model for multi-stage early arc-forearc magmatism in
347 Tethyan subduction factories: *Lithos*, v. 113, no. 1, p. 68-87.

348 Escrig, S., Bézou, A., Langmuir, C., Michael, P., and Arculus, R., 2012, Characterizing the effect
349 of mantle source, subduction input and melting in the Fonualei Spreading Center, Lau
350 Basin: Constraints on the origin of the boninitic signature of the back- arc lavas:
351 *Geochemistry, Geophysics, Geosystems*, v. 13, no. 10.

352 Falloon, T. J., and Crawford, A. J., 1991, The petrogenesis of high-calcium boninite lavas
353 dredged from the northern Tonga ridge: *Earth and Planetary Science Letters*, v. 102, no.
354 3-4, p. 375-394.

355 Falloon, T. J., Danyushevsky, L. V., Crawford, A. J., Meffre, S., Woodhead, J. D., and Bloomer,
356 S. H., 2008, Boninites and adakites from the northern termination of the Tonga Trench:
357 implications for adakite petrogenesis: *Journal of Petrology*, v. 49, no. 4, p. 697-715.

358 Falloon, T. J., Danyushevsky, L. V., Crawford, T. J., Maas, R., Woodhead, J. D., Eggins, S. M.,
359 Bloomer, S. H., Wright, D. J., Zlobin, S. K., and Stacey, A. R., 2007, Multiple mantle
360 plume components involved in the petrogenesis of subduction- related lavas from the
361 northern termination of the Tonga Arc and northern Lau Basin: Evidence from the
362 geochemistry of arc and backarc submarine volcanics: *Geochemistry, Geophysics,*
363 *Geosystems*, v. 8, no. 9.

364 Falloon, T. J., Green, D. H., and Crawford, A., 1987, Dredged igneous rocks from the northern
365 termination of the Tofua magmatic arc, Tonga and adjacent Lau Basin: *Australian*
366 *Journal of Earth Sciences*, v. 34, no. 4, p. 487-506.

367 Falloon, T. J., Green, D. H., and McCulloch, M., 1989, Petrogenesis of high-Mg and associated
368 lavas from the north Tonga trench, p. 357-395.

369 Flower, M. F., and Levine, H. M., 1987, Petrogenesis of a tholeiite-boninite sequence from
370 Ayios Mamas, Troodos ophiolite: evidence for splitting of a volcanic arc?: *Contributions*
371 *to Mineralogy and Petrology*, v. 97, no. 4, p. 509-524.

372 Gale, A., Dalton, C. A., Langmuir, C. H., Su, Y., and Schilling, J. G., 2013, The mean
373 composition of ocean ridge basalts: *Geochemistry, Geophysics, Geosystems*, v. 14, no. 3,
374 p. 489-518.

1
2
3
4 375 Gass, I., 1968, Is the Troodos massif of Cyprus a fragment of Mesozoic ocean floor?: *Nature*, v.
5 376 220, p. 39-42.
6
7 377 Gass, I. G., MacLeod, C. J., Murton, B., Panayiotou, A., Simonian, K., and Xenophontos, C.,
8 378 1994, The geological evolution of the Southern Troodos transform fault zone, Geological
9 379 Survey Department, v. 9.
10 380 Hickey-Vargas, R., Yogodzinski, G., Ishizuka, O., McCarthy, A., Bizimis, M., Kusano, Y.,
11 381 Savov, I., and Arculus, R., 2018, Origin of depleted basalts during subduction initiation
12 382 and early development of the Izu-Bonin-Mariana island arc: Evidence from IODP
13 383 expedition 351 site U1438, Amami-Sankaku basin: *Geochimica et Cosmochimica Acta*,
14 384 v. 229, p. 85-111.
15
16 385 Ishizuka, O., Hickey-Vargas, R., Arculus, R. J., Yogodzinski, G. M., Savov, I. P., Kusano, Y.,
17 386 McCarthy, A., Brandl, P. A., and Sudo, M., 2018, Age of Izu–Bonin–Mariana arc
18 387 basement: *Earth and Planetary Science Letters*, v. 481, p. 80-90.
19
20 388 Ishizuka, O., Kimura, J.-I., Li, Y. B., Stern, R. J., Reagan, M. K., Taylor, R. N., Ohara, Y.,
21 389 Bloomer, S. H., Ishii, T., and Hargrove, U. S., 2006, Early stages in the evolution of Izu–
22 390 Bonin arc volcanism: New age, chemical, and isotopic constraints: *Earth and Planetary*
23 391 *Science Letters*, v. 250, no. 1, p. 385-401.
24
25 392 Ishizuka, O., Tani, K., and Reagan, M. K., 2014, Izu-Bonin-Mariana forearc crust as a modern
26 393 ophiolite analogue: *Elements*, v. 10, no. 2, p. 115-120.
27
28 394 Ishizuka, O., Tani, K., Reagan, M. K., Kanayama, K., Umino, S., Harigane, Y., Sakamoto, I.,
29 395 Miyajima, Y., Yuasa, M., and Dunkley, D. J., 2011, The timescales of subduction
30 396 initiation and subsequent evolution of an oceanic island arc: *Earth and Planetary Science*
31 397 *Letters*, v. 306, no. 3, p. 229-240.
32
33 398 Karsten, J., Klein, E., and Sherman, S., 1996, Subduction zone geochemical characteristics in
34 399 ocean ridge basalts from the southern Chile Ridge: implications of modern ridge
35 400 subduction systems for the Archean: *Lithos*, v. 37, no. 2-3, p. 143-161.
36
37 401 Keller, N. S., Arculus, R. J., Hermann, J., and Richards, S., 2008, Submarine back- arc lava with
38 402 arc signature: Fonualei Spreading Center, northeast Lau Basin, Tonga: *Journal of*
39 403 *Geophysical Research: solid earth*, v. 113, no. B8.
40
41 404 König, S., Münker, C., Schuth, S., Luguët, A., Hoffmann, J. E., and Kuduon, J., 2010, Boninites
42 405 as windows into trace element mobility in subduction zones: *Geochimica et*
43 406 *Cosmochimica Acta*, v. 74, no. 2, p. 684-704.
44
45 407 Langmuir, C., Bezos, A., Escrig, S., and Parman, S., 2006, Chemical systematics and hydrous
46 408 melting of the mantle in back- arc basins: *Back-Arc Spreading Systems: Geological,*
47 409 *Biological, Chemical, and Physical Interactions*, p. 87-146.
48
49 410 Le Bas, M., 2000, IUGS reclassification of the high-Mg and picritic volcanic rocks: *Journal of*
50 411 *Petrology*, v. 41, no. 10, p. 1467-1470.
51
52 412 Le Voci, G., Davies, D., Goes, S., Kramer, S. C., and Wilson, C. R., 2014, A systematic 2- D
53 413 investigation into the mantle wedge's transient flow regime and thermal structure:
54 414 Complexities arising from a hydrated rheology and thermal buoyancy: *Geochemistry,*
55 415 *Geophysics, Geosystems*, v. 15, no. 1, p. 28-51.
56
57 416 Maffione, M., Hinsbergen, D. J., Gelder, G. I., Goes, F. C., and Morris, A., 2017, Kinematics of
58 417 Late Cretaceous subduction initiation in the Neo- Tethys Ocean reconstructed from
59 418 ophiolites of Turkey, Cyprus, and Syria: *Journal of Geophysical Research: Solid Earth*, v.
60 419 122, no. 5, p. 3953-3976.
61
62
63
64
65

1
2
3
4
5
6
7
8
9
10
11
12
13
14
15
16
17
18
19
20
21
22
23
24
25
26
27
28
29
30
31
32
33
34
35
36
37
38
39
40
41
42
43
44
45
46
47
48
49
50
51
52
53
54
55
56
57
58
59
60
61
62
63
64
65

420 McDonough, W. F., and Sun, S.-S., 1995, The composition of the Earth: Chemical geology, v.
421 120, no. 3, p. 223-253.

422 McKenzie, D. P., and Morgan, W., 1969, Evolution of triple junctions: Nature, v. 224, no. 5215,
423 p. 125.

424 Miyashiro, A., 1974, Volcanic rock series in island arcs and active continental margins:
425 American Journal of Science, v. 274, no. 4, p. 321-355.

426 Moores, E., Robinson, P. T., Malpas, J., and Xenophonotos, C., 1984, Model for the origin of the
427 Troodos massif, Cyprus, and other mideast ophiolites: Geology, v. 12, no. 8, p. 500-503.

428 Moores, E., and Vine, F., 1971, The Troodos Massif, Cyprus and other ophiolites as oceanic
429 crust: evaluation and implications: Philosophical Transactions of the Royal Society of
430 London A: Mathematical, Physical and Engineering Sciences, v. 268, no. 1192, p. 443-
431 467.

432 Mukasa, S. B., and Ludden, J. N., 1987, Uranium-lead isotopic ages of plagiogranites from the
433 Troodos ophiolite, Cyprus, and their tectonic significance: Geology, v. 15, no. 9, p. 825-
434 828.

435 Osozawa, S., Shinjo, R., Lo, C.-H., Jahn, B.-m., Hoang, N., Sasaki, M., Ishikawa, K. i., Kano,
436 H., Hoshi, H., and Xenophonotos, C., 2012, Geochemistry and geochronology of the
437 Troodos ophiolite: An SSZ ophiolite generated by subduction initiation and an extended
438 episode of ridge subduction?: Lithosphere, v. 4, no. 6, p. 497-510.

439 Pearce, J., 1975, Basalt geochemistry used to investigate past tectonic environments on Cyprus:
440 Tectonophysics, v. 25, no. 1-2, p. 41-67.

441 Pearce, J., and Robinson, P., 2010, The Troodos ophiolitic complex probably formed in a
442 subduction initiation, slab edge setting: Gondwana Research, v. 18, no. 1, p. 60-81.

443 Pearce, J. A., Ernewein, M., Bloomer, S. H., Parson, L. M., Murton, B. J., and Johnson, L. E.,
444 1994, Geochemistry of Lau Basin volcanic rocks: influence of ridge segmentation and arc
445 proximity: Geological Society, London, Special Publications, v. 81, no. 1, p. 53-75.

446 Pearce, J. A., Lippard, S., and Roberts, S., 1984, Characteristics and tectonic significance of
447 supra-subduction zone ophiolites: Geological Society, London, Special Publications, v.
448 16, no. 1, p. 77-94.

449 Pearce, J. A., Reagan, M. K., Petronotis, K., Morgan, S., Almeev, R., Avery, A. J., Carvallo, C.,
450 Chapman, T., Christeson, G. L., and Ferré, E. C., 2015, Izu-Bonin-Mariana fore arc:
451 Testing subduction initiation and ophiolite models by drilling the outer Izu-Bonin-
452 Mariana fore arc; 30 July–29 September 2014: Integrated Ocean Drilling Program:
453 Preliminary Reports, v. 352.

454 Peate, D. W., Kokfelt, T. F., Hawkesworth, C. J., Van Calsteren, P. W., Hergt, J. M., and Pearce,
455 J. A., 2001, U-series isotope data on Lau Basin glasses: The role of subduction-related
456 fluids during melt generation in back-arc basins: Journal of Petrology, v. 42, no. 8, p.
457 1449-1470.

458 Peate, D. W., Pearce, J. A., Hawkesworth, C. J., Colley, H., Edwards, C. M., and Hirose, K.,
459 1997, Geochemical variations in Vanuatu arc lavas: the role of subducted material and a
460 variable mantle wedge composition: Journal of Petrology, v. 38, no. 10, p. 1331-1358.

461 Rautenschlein, M., Jenner, G., Hertogen, J., Hofmann, A., Kerrich, R., Schmincke, H.-U., and
462 White, W., 1985, Isotopic and trace element composition of volcanic glasses from the
463 Akaki Canyon, Cyprus: implications for the origin of the Troodos ophiolite: Earth and
464 Planetary Science Letters, v. 75, no. 4, p. 369-383.

1
2
3
4
5
6
7
8
9
10
11
12
13
14
15
16
17
18
19
20
21
22
23
24
25
26
27
28
29
30
31
32
33
34
35
36
37
38
39
40
41
42
43
44
45
46
47
48
49
50
51
52
53
54
55
56
57
58
59
60
61
62
63
64
65

465 Reagan, M. K., Ishizuka, O., Stern, R. J., Kelley, K. A., Ohara, Y., Blichert-Toft, J., Bloomer,
466 S. H., Cash, J., Fryer, P., and Hanan, B. B., 2010, Fore-arc basalts and subduction
467 initiation in the Izu-Bonin-Mariana system: *Geochemistry, Geophysics, Geosystems*, v.
468 11, no. 3.

469 Reagan, M. K., Pearce, J. A., Petronotis, K., Almeev, R. R., Avery, A. J., Carvalho, C., Chapman,
470 T., Christeson, G. L., Ferré, E. C., and Godard, M., 2017, Subduction initiation and
471 ophiolite crust: new insights from IODP drilling: *International Geology Review*, v. 59,
472 no. 11, p. 1439-1450.

473 Regelous, M., Haase, K., Freund, S., Keith, M., Weinzierl, C., Beier, C., Brandl, P., Endres, T.,
474 and Schmidt, H., 2014, Formation of the Troodos Ophiolite at a triple junction: Evidence
475 from trace elements in volcanic glass: *Chemical Geology*, v. 386, p. 66-79.

476 Resing, J. A., Rubin, K. H., Embley, R. W., Lupton, J. E., Baker, E. T., Dziak, R. P.,
477 Baumberger, T., Lilley, M. D., Huber, J. A., and Shank, T. M., 2011, Active submarine
478 eruption of boninite in the northeastern Lau Basin: *Nature Geoscience*, v. 4, no. 11, p.
479 799-806.

480 Robertson, A. H., 2002, Overview of the genesis and emplacement of Mesozoic ophiolites in the
481 Eastern Mediterranean Tethyan region: *Lithos*, v. 65, no. 1, p. 1-67.

482 Robinson, P. T., Malpas, J., Xenophontos, C., Dilek, Y., and Newcomb, S., 2003, The Troodos
483 massif of Cyprus: Its role in the evolution of the ophiolite concept: *Special papers-*
484 *Geological Society of America*, p. 295-308.

485 Robinson, P. T., Melson, W. G., O'Hearn, T., and Schmincke, H.-U., 1983, Volcanic glass
486 compositions of the Troodos ophiolite, Cyprus: *Geology*, v. 11, no. 7, p. 400-404.

487 Sharaskin, A. Y., Karpenko, S., Ljalikov, A., Zlobin, S., and Balashov, Y., 1983, Correlated
488 $^{143}\text{Nd}/^{144}\text{Nd}$ and $^{87}\text{Sr}/^{86}\text{Sr}$ data on boninites from Mariana and Tonga arcs: *Ophioliti*, v.
489 8, no. 3, p. 431-438.

490 Sigurdsson, I., Kamenetsky, V., Crawford, A., Eggins, S., and Zlobin, S., 1993, Primitive island
491 arc and oceanic lavas from the Hunter ridge-Hunter fracture zone. Evidence from glass,
492 olivine and spinel compositions: *Mineralogy and Petrology*, v. 47, no. 2-4, p. 149-169.

493 Stern, R. J., Reagan, M., Ishizuka, O., Ohara, Y., and Whattam, S., 2012, To understand
494 subduction initiation, study forearc crust: To understand forearc crust, study ophiolites:
495 *Lithosphere*, v. 4, no. 6, p. 469-483.

496 Syracuse, E. M., and Abers, G. A., 2006, Global compilation of variations in slab depth beneath
497 arc volcanoes and implications: *Geochemistry, Geophysics, Geosystems*, v. 7, no. 5.

498 Whattam, S. A., and Stern, R. J., 2011, The 'subduction initiation rule': a key for linking
499 ophiolites, intra-oceanic forearcs, and subduction initiation: *Contributions to Mineralogy*
500 *and Petrology*, v. 162, no. 5, p. 1031-1045.

501 Woelki, D., Regelous, M., Haase, K. M., Romer, R. H., and Beier, C., 2018, Petrogenesis of
502 boninitic lavas from the Troodos Ophiolite, and comparison with Izu-Bonin-Mariana
503 fore-arc crust: *Earth and Planetary Science Letters*, v. 498, p. 203-214.

1
2
3
4
5
6
7
8
9
10
11
12
13
14
15
16
17
18
19
20
21
22
23
24
25
26
27
28
29
30
31
32
33
34
35
36
37
38
39
40
41
42
43
44
45
46
47
48
49
50
51
52
53
54
55
56
57
58
59
60
61
62
63
64
65

508 Figure captions

509 Figure 1. Simplified geological map of the Troodos Ophiolite (modified from Osozawa et al.
510 (2012)), showing sample locations (grey dots), profiles through the extrusive series (black lines)
511 and the three areas (NM, SWM, SEM) defined on the basis of trace element composition.

512
513 Figure 2. Major element variations (MgO, SiO₂ and TiO₂) in volcanic glasses from the Troodos
514 Ophiolite. Data are from this study, Akaki (Regelous et al., 2014) and Parekkklisia (Woelki et al.,
515 2018). Fields defined for boninites (BON) are based on the classification of Le Bas (2000).
516 Based on this classification, boninites are restricted to the SWM and SEM glasses.

517
518 Figure 3. Trace element composition of Troodos glasses normalized to N-MORB (McDonough
519 and Sun, 1995). All NM, SWM and SEM glasses (data from this study and Regelous et al.
520 (2014); Woelki et al. (2018)) are enriched in fluid mobile elements Cs, Rb, Ba, U, Pb and Sr,
521 compared to less mobile elements of similar incompatibility. The mean Troodos boninite
522 composition is based on 142 analyses from this work and from Woelki et al. (2018). Note the
523 relatively high Zr and Hf compared to Sm and Eu in IBM boninites (Reagan et al., 2010),
524 compared to boninites from Troodos and from young back-arc (Falloon and Crawford, 1991;
525 Falloon et al., 2008; Falloon et al., 2007; Falloon et al., 1989) and arc (Cooper et al., 2010)
526 settings.

527
528 Figure 4. A. Variation in glass composition with distance from the lava-sediment boundary as
529 determined from the geological map of Cyprus (Constantinou, 1995) for seven different sections
530 through the Troodos lava sequence. The bar represents mean composition for each section. Note

1
2
3
4
5
6
7
8
9
10
11
12
13
14
15
16
17
18
19
20
21
22
23
24
25
26
27
28
29
30
31
32
33
34
35
36
37
38
39
40
41
42
43
44
45
46
47
48
49
50
51
52
53
54
55
56
57
58
59
60
61
62
63
64
65

531 that most sections show no systematic geochemical variation with relative stratigraphic age.
532 Instead, glasses from the northern margin (NM) have higher Zr/Yb ratios than glasses from the
533 southern margin (SWM, SEM), indicating that those from the northern margin were derived
534 from a less depleted mantle source. B. Box-whisker plot of Ba/Ce ratios for glasses from the
535 seven sections, with whiskers extended to most extreme data points. Glasses from the southern
536 margin (SWM, SEM) have higher Ba/Ce than glasses from the northern margin.

537
538 Figure 5. Variation of Ce/Pb with Zr/Yb in Troodos glasses, compared with lavas from (A) the
539 IBM fore-arc (Hickey-Vargas et al., 2018; Ishizuka et al., 2018; Ishizuka et al., 2011; Reagan et
540 al., 2010), and (B) the Tonga-Lau arc – back-arc system. Troodos data are from Regelous et al.
541 (2014); Woelki et al. (2018) and this study. (A) Troodos NM glasses overlap in composition with
542 some IBM lavas, but extend to far lower Zr/Yb ratios. Troodos glasses define positive
543 correlations between Zr/Yb and Ce/Pb, in contrast to the negative correlation for IBM fore-arc
544 lavas. (B) The Zr/Yb and Ce/Pb ratios of Troodos NM glasses overlap with Fonualei Rift back-
545 arc lavas (Escrig et al., 2012) (dashed field) indicating similar degree of mantle depletion and
546 subduction enrichment. The Ce/Pb and Zr/Yb ratios of SWM and SEM glasses partly overlap
547 with Tofua island arc lavas (Caulfield et al., 2012b), but extend to lower Ce/Pb and Zr/Yb. Data
548 for Eastern Lau and Central Lau Spreading Centre lavas from Bézos et al. (2009); Pearce et al.
549 (1994); Peate et al. (2001), MORB data from Jenner and O’Neill, 2012, Valu Fa Ridge data are
550 from Bach et al. (1998), Tonga boninite data are from Cooper et al. (2010); Falloon and
551 Crawford (1991); Falloon et al. (2008); Falloon et al. (2007); Falloon et al. (1989).

552

1
2
3
4
5
6
7
8
9
10
11
12
13
14
15
16
17
18
19
20
21
22
23
24
25
26
27
28
29
30
31
32
33
34
35
36
37
38
39
40
41
42
43
44
45
46
47
48
49
50
51
52
53
54
55
56
57
58
59
60
61
62
63
64
65

553 Figure 6. Distance to arc (km) plotted against Zr/Yb and Ce/Pb ratios of Tonga – Lau Basin
554 glasses. Distance to arc in the Tonga arc-back-arc system measured by GeoMapApp®
555 application (<http://www.geomapapp.org/>). Mantle wedge depletion (decreasing Zr/Yb) and
556 subduction component enrichment (decreasing Ce/Pb) increases with decreasing distance to the
557 arc for the Tonga back-arc system (Bach et al., 1998; Bézos et al., 2009; Escrig et al., 2012;
558 Pearce et al., 1994; Peate et al., 1997). The boxes of Troodos glasses represent box-whisker plots
559 extended to the most extreme values and compared distances of the Fonualei spreading centre
560 (Escrig et al., 2012). The NM glasses overlap with Fonualei Spreading centre lavas, which are 25
561 – 75 km away from the active arc. Compositional field of the Troodos NM, SWM and SEM
562 indicate a distance less than 75 km to the “arc” position.

563
564 Figure 7. Ti_8 and Fe_8 (TiO_2 and FeO contents fractionation corrected to $MgO = 8$ wt%, based on
565 the liquid line of descent) of the Troodos glasses. Only glasses >5 wt% MgO are used for
566 correction. Data are from this study and Regelous et al. (2014); Woelki et al. (2018). Shown for
567 comparison are global MORB (Gale et al., 2013), Fonualei Spreading Centre (Escrig et al., 2012)
568 and ELSC glasses (grey field) (Bézos et al., 2009). Troodos glasses overlap with back-arc lava
569 trends of the ELSC and Fonualei spreading centre towards lower Ti_8 and Fe_8 values. Grey
570 symbols for melting conditions are from Langmuir et al. (2006).

571
572 Figure 8. Inferred position and orientation of the former subduction zone beneath the Troodos
573 Ophiolite, with the Troodos Ophiolite rotated 90° clockwise to its orientation at 91 Ma. Red
574 dashed lines indicate approximate distance to slab surface inferred from comparison with global
575 arc and back-arc systems including the Tonga-Lau system (Caulfield et al., 2012a; Escrig et al.,

1
2
3
4
5
6
7
8
9
10
11
12
13
14
15
16
17
18
19
20
21
22
23
24
25
26
27
28
29
30
31
32
33
34
35
36
37
38
39
40
41
42
43
44
45
46
47
48
49
50
51
52
53
54
55
56
57
58
59
60
61
62
63
64
65

576 2012; Keller et al., 2008; Syracuse and Abers, 2006). Blue lines are parallel to the former
577 Troodos spreading axis, with arrows indicating spreading direction on the basis of sheeted dyke
578 orientations (Maffione et al., 2017). Black line represents the Arakapas Fault Zone (Gass et al.,
579 1994).

580

581

Figure 1

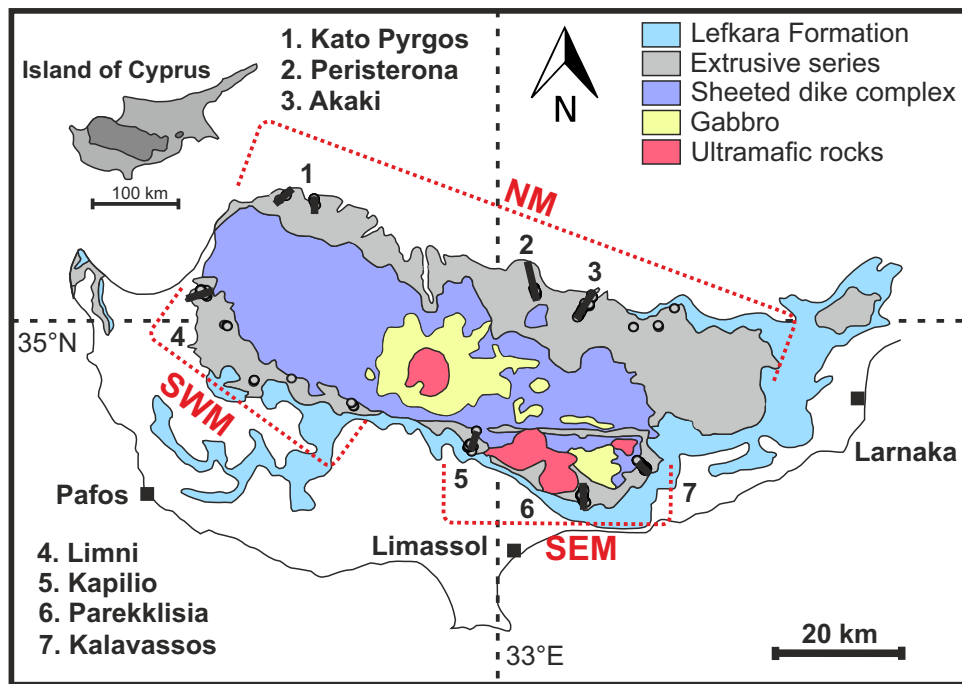


Figure 2

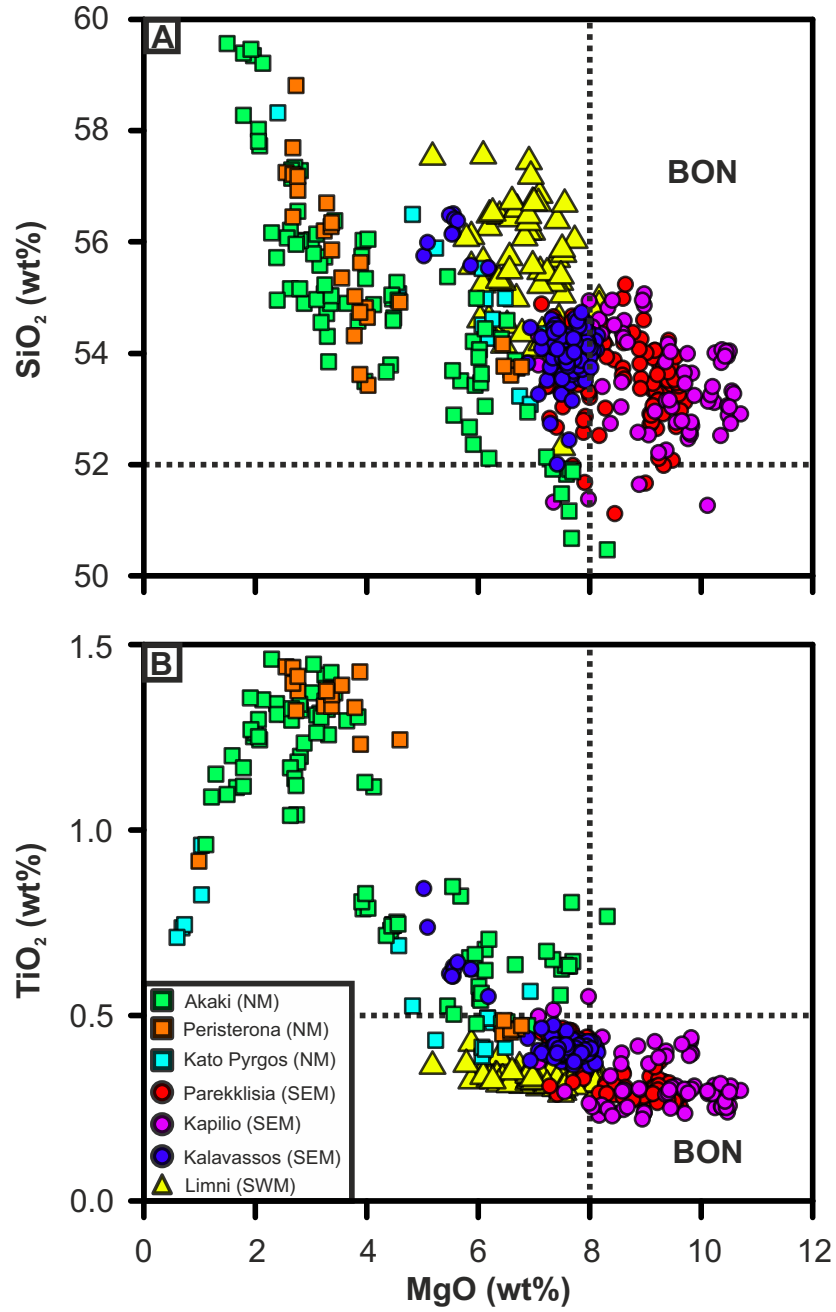


Figure 3

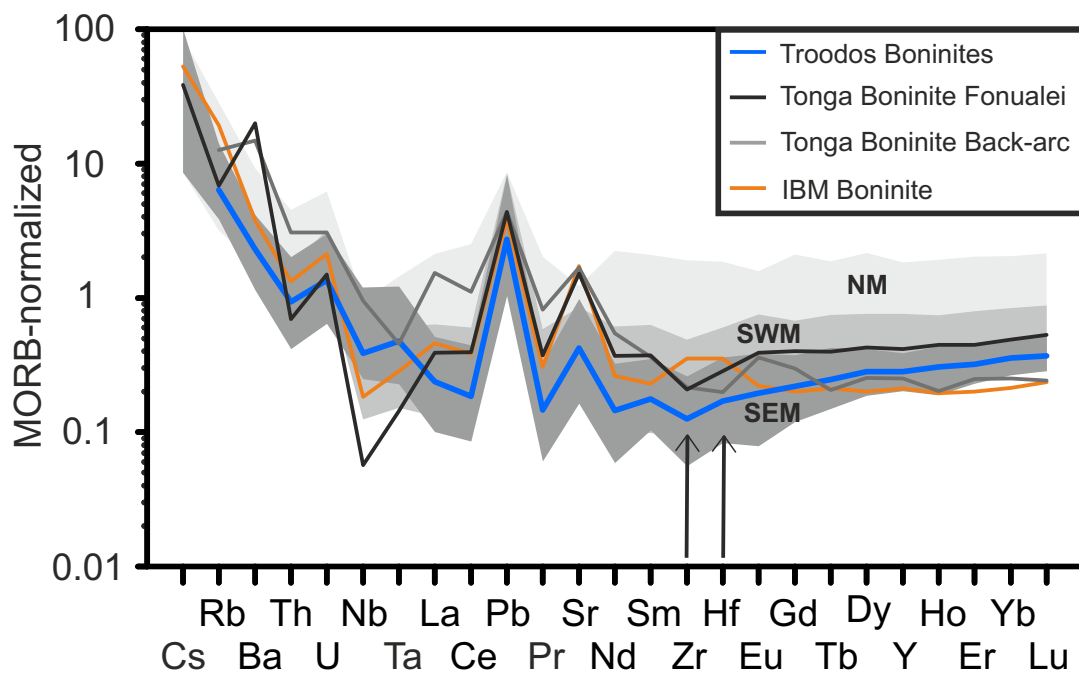


Figure 4

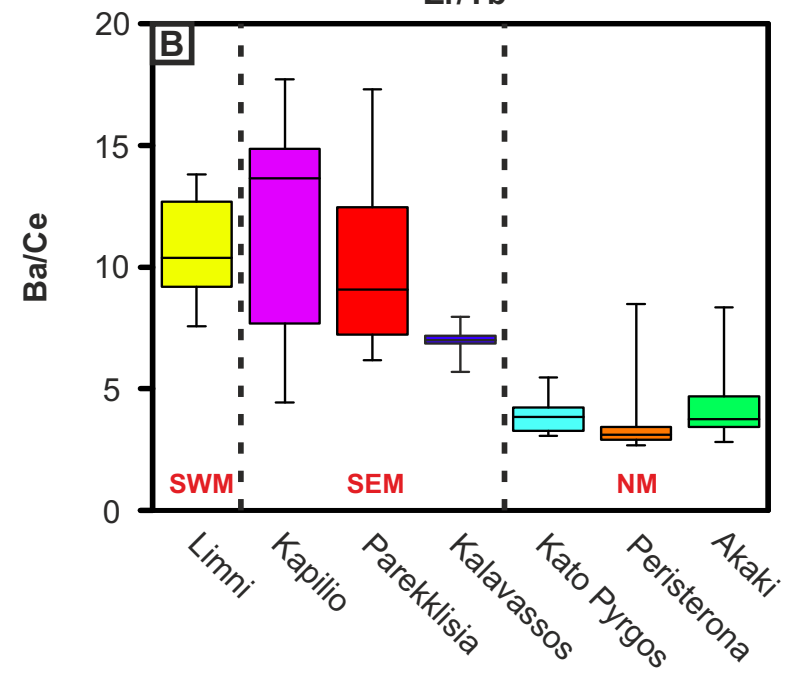
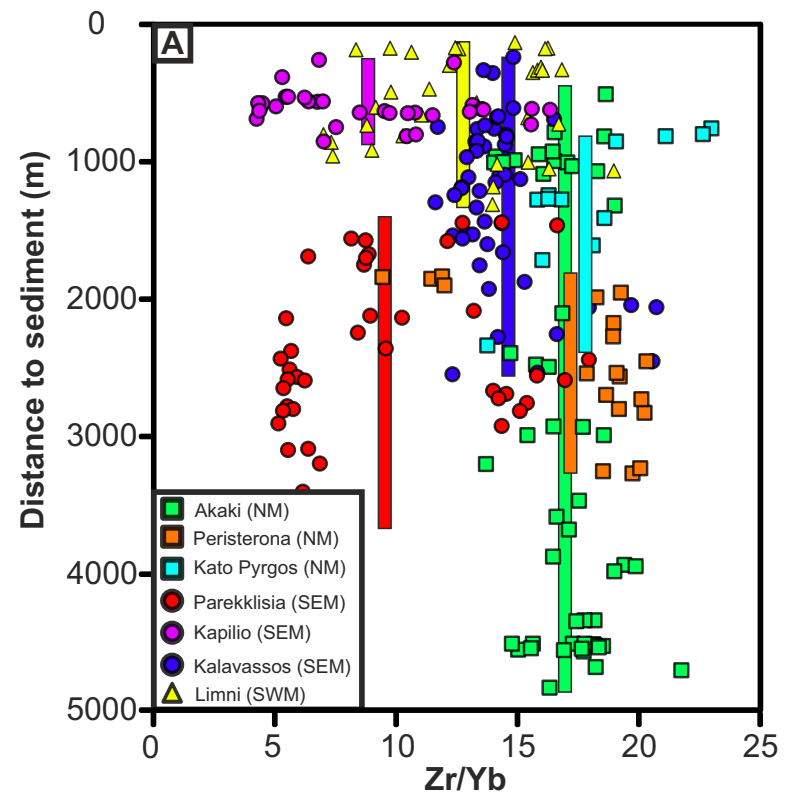


Figure 5

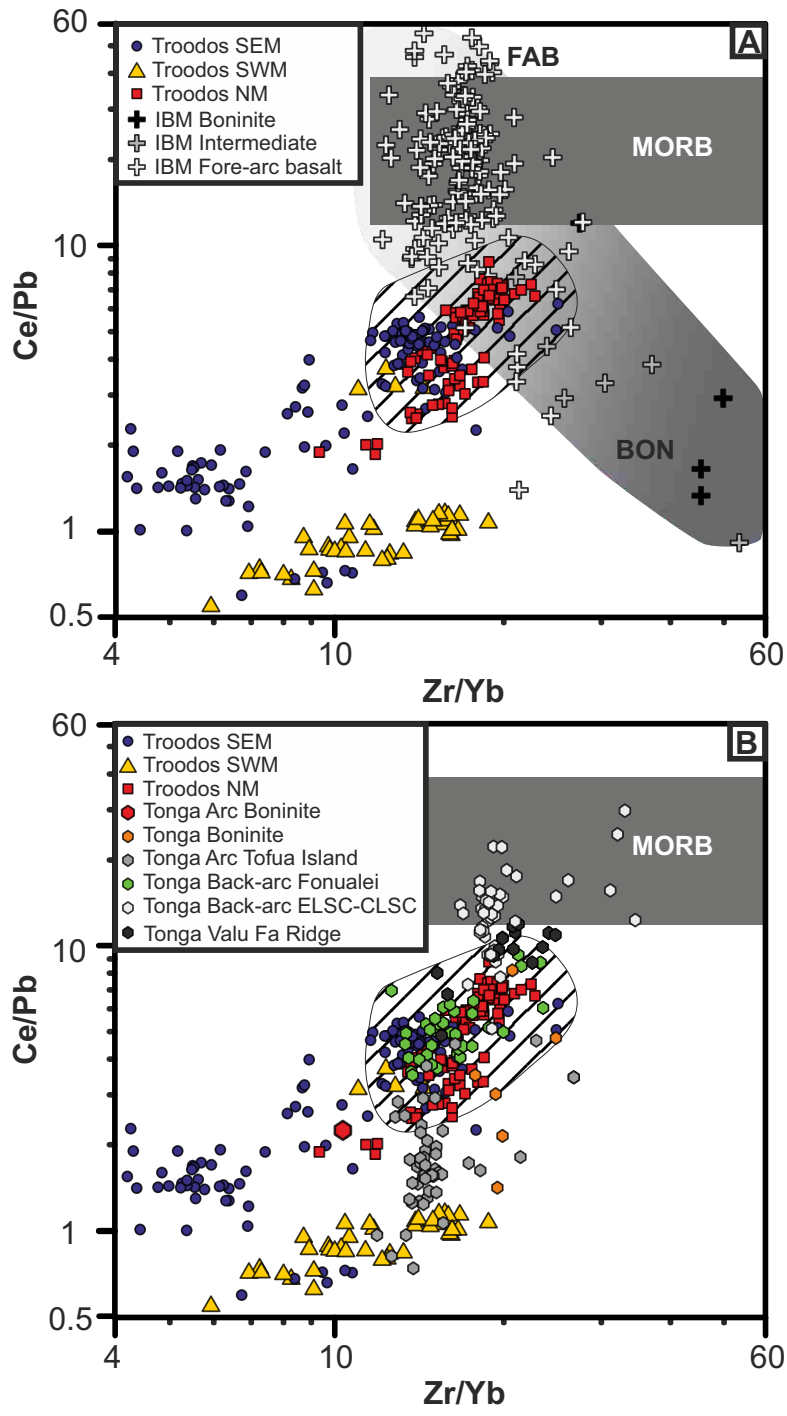


Figure 6

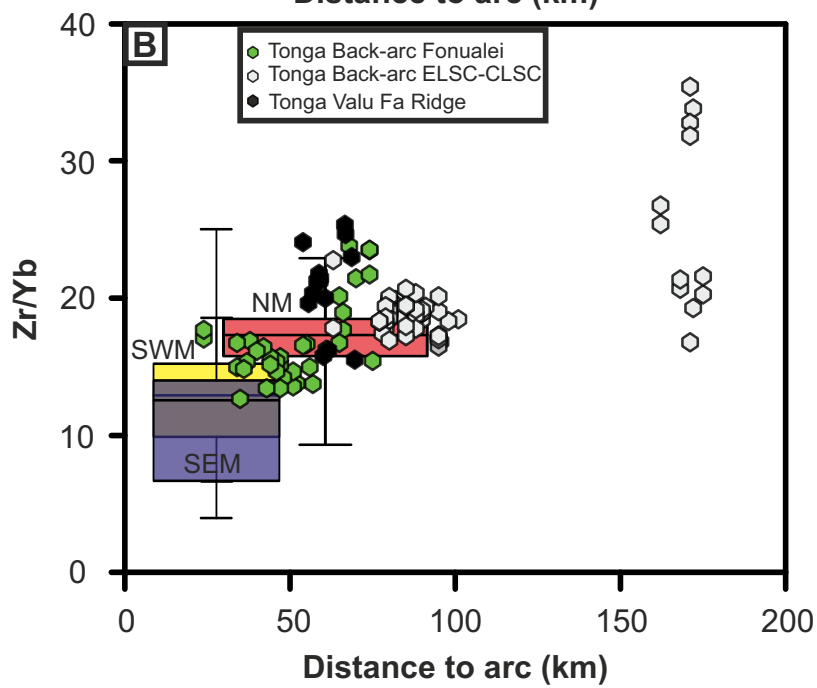
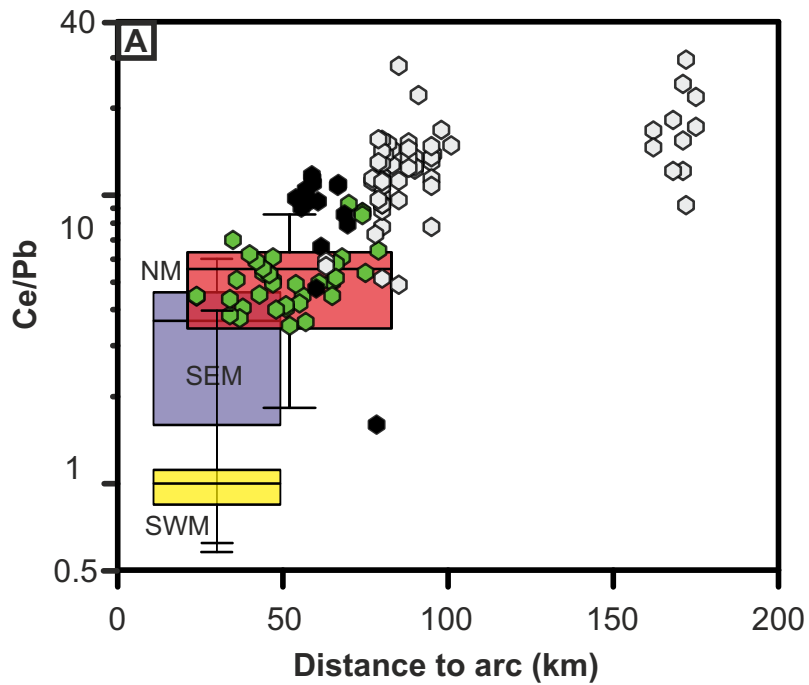


Figure 7

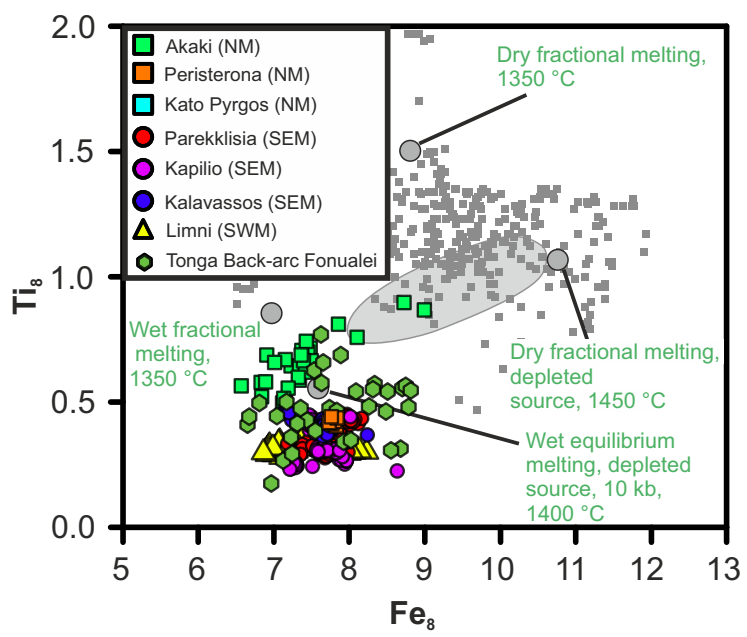


Figure 8

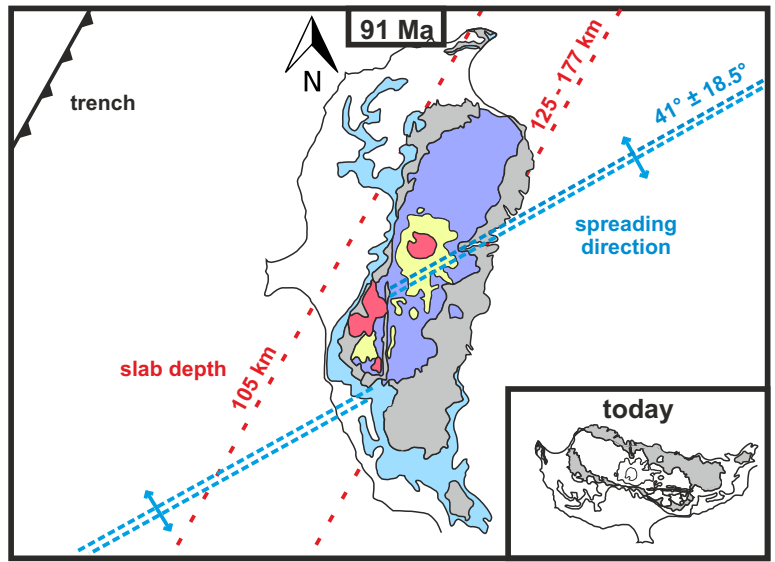


Figure S1

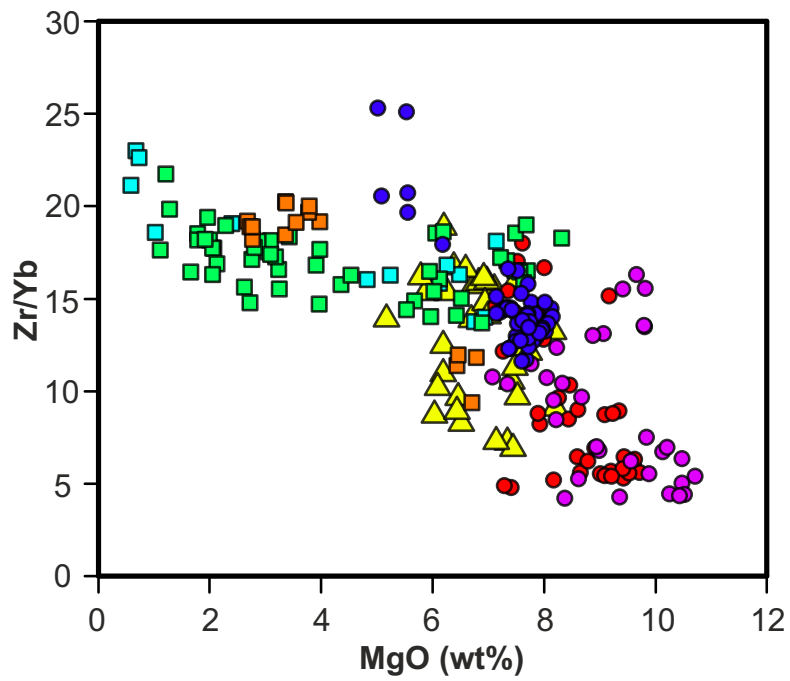


Figure S1. Variation of Zr/Yb with MgO (wt%) for Troodos glasses. There is no systematic variation of Zr/Yb with MgO for each individual group, indicating source variation rather than crystal fractionation or crustal assimilation.

TABLE S1. MAJOR (WT%) AND TRACE ELEMENT (PPM) COMPOSITION OF TROOL

Sample #	IGSN sample #	Rock Type	Locality
CY16-GLASS-1	IEGZN0001	Tholeiite	Limni
CY16-GLASS-2	IEGZN0002	Tholeiite	Limni
CY16-GLASS-3	IEGZN0003	Tholeiite	Limni
CY16-GLASS-11	IEGZN0004	Tholeiite	Limni
CY16-GLASS-12	IEGZN0005	Tholeiite	Limni
CY16-GLASS-14	IEGZN0006	Boninite	Limni
CY16-GLASS-19	IEGZN0007	Tholeiite	Limni
CY16-GLASS-20	IEGZN0008	Tholeiite	Limni
CY16-GLASS-21	IEGZN0009	Tholeiite	Limni
CY16-GLASS-23	IEGZN0010	Tholeiite	Limni
CY16-GLASS-24	IEGZN0011	Tholeiite	Limni
CY16-GLASS-25	IEGZN0012	Tholeiite	Limni
CY16-GLASS-26	IEGZN0013	Tholeiite	Limni
CY16-GLASS-27	IEGZN0014	Tholeiite	Limni
CY16-GLASS-28	IEGZN0015	Tholeiite	Limni
CY16-GLASS-29	IEGZN0016	Boninite	Limni
CY16-GLASS-30	IEGZN0017	Boninite	Limni
Cy16-GLASS-31	IEGZN0018	Boninite	Limni
CY16-GLASS-32	IEGZN0019	Tholeiite	Limni
CY16-GLASS-33	IEGZN0020	Tholeiite	Limni
CY16-GLASS-34	IEGZN0021	Tholeiite	Limni
CY16-GLASS-35	IEGZN0022	Tholeiite	Limni
CY16-GLASS-36	IEGZN0023	Tholeiite	Limni
CY16-GLASS-37	IEGZN0024	Tholeiite	Limni
CY16-GLASS-38	IEGZN0025	Tholeiite	Limni
CY16-GLASS-39	IEGZN0026	Tholeiite	Limni
CY16-GLASS-40	IEGZN0027	Tholeiite	Limni
CY16-GLASS-42	IEGZN0028	Tholeiite	Limni
CY16-GLASS-43	IEGZN0029	Tholeiite	Limni
CY16-GLASS-44	IEGZN0030	Tholeiite	Limni
CY1601	IEGZN0031	Boninite	Limni
CY1603	IEGZN0032	Tholeiite	Limni
CY1604	IEGZN0033	Tholeiite	Limni
CY1606	IEGZN0034	Tholeiite	Limni
CY1608	IEGZN0035	Tholeiite	Limni
CY1610	IEGZN0036	Tholeiite	Limni
CY1611	IEGZN0037	Tholeiite	Limni
CY1612	IEGZN0038	Tholeiite	Limni
CY1613	IEGZN0039	Tholeiite	Limni
CY1614	IEGZN0040	Tholeiite	Limni
CY1616	IEGZN0041	Tholeiite	Limni
CY1617	IEGZN0042	Tholeiite	Limni
CY1619	IEGZN0043	Tholeiite	Limni
CY1620	IEGZN0044	Tholeiite	Limni
CY1621	IEGZN0045	Tholeiite	Limni
CY1622	IEGZN0046	Tholeiite	Limni
CY1623	IEGZN0047	Boninite	Limni